Ocean Dynamics
https://doi.org/10.1007/s10236-020-01424-x

Long-term observations of the group structure of surface waves in ice

Johannes Gemmrich[1] · Todd Mudge[2] · Jim Thomson[3]

Received: 13 June 2020 / Accepted: 9 November 2020

Abstract
Several years of surface wave observations in the Chukchi Sea reveal wave groups are a common feature in open water and ice-covered conditions. The strength of the groupiness, here characterized by the group factor, is well correlated with the characteristic wave steepness, the spectral bandwidth, and the Benjamin-Feir Index. The general finding is enhanced groupiness in ice. However, the trends with wave characteristics are opposite from ice to open water, and suggest different mechanisms. In ice, groupiness increases with decreasing steepness, increasing bandwidth, and decreasing Benjamin-Feir Index. In open water, the trends indicate that both linear superposition of phase-coherent waves and nonlinear behaviour are important for the generation of wave groups. We hypothesize that in ice-covered conditions, directional spreading reduces the effective bandwidth in the dominant wave direction, possibly due to modified four-wave nonlinear transfer spreading high-frequency energy to lateral directions. This reduced effective bandwidth is then conducive to enhanced group formation by linear superposition. However, an increased high-frequency noise floor of the in-ice observations would also be consistent with the observed increase in omni-directional bandwidth. Without directional measurements, neither of these two processes can be favoured with certainty.

Keywords Wave groups in ice · Nonlinear waves · Directional waves

1 Introduction

Groups or 'sets' of waves that are larger in amplitude than the background wave field are a common phenomenon in ocean surface wave measurements in both deep (Longuet-Higgins 1984) and shallow (Elgar et al. 1984) waters. Wave groups are important to breaking (Banner and Pierson 2007), the emergence of rogue waves (Gemmrich and Thomson 2017), Lagrangian transport of material at the ocean surface (van den Bremer and Taylor 2015), and air-sea fluxes (Sullivan et al. 2018). The groups can form from both linear and nonlinear mechanisms. In the linear mechanism, the linear superposition of two wave trains of frequency ω_1 and $\omega_2 = \omega_1 + \Delta\omega$ generates a regular train of wave groups with a frequency of the groups equal $\Delta\omega$. This 'beat' frequency also occurs in cases of irregular waves with frequencies spanning a range ω, though the effects are less coherent. The nonlinear mechanisms include focusing and modulational instability (Benjamin and Feir 1967), which is a four-wave interaction that can make a narrow-banded wave spectrum unstable.

Wave groups are particularly interesting in the presence of sea ice, because both linear and nonlinear mechanisms may be altered. The linear mechanism is likely to be altered by a narrowing of the wave frequency spectrum (i.e. reduced range of ω) in sea ice, which is the result of preferential wave attenuation at higher frequencies (Shen and Squire 1998; Rogers et al. 2016; Cheng et al. 2017; Meylan et al. 2018). The nonlinear mechanism may be altered in sea ice, via changes to the wave dispersion relation that enhance four-wave interactions and instabilities (Liu and Mollo-Christensen 1988; Polnikov and Lavrenov 2007).

Responsible Editor: Amin Chabchoub

This article is part of the Topical Collection on the *16th International Workshop on Wave Hindcasting and Forecasting in Melbourne, AU, November 10-15, 2019*

✉ Johannes Gemmrich
gemmrich@uvic.ca

[1] University of Victoria, Physics & Astronomy, Victoria, BC, Canada

[2] ASL Environmental Sciences, Victoria, BC, Canada

[3] Applied Physics Laboratory, University of Washington, Seattle, WA, USA

Recently, two field studies have explored wave groups in the marginal ice zone (MIZ), where waves impinge on sea ice from open water. Collins et al. (2015) used observations from the Barents Sea to show that wave groups were enhanced in thick ($1 - 3$ m) sea ice and concluded that nonlinear mechanisms were important. Thomson et al. (2019) used observations from the Beaufort Sea to show that wave groups were enhanced in thin (< 0.5 m) sea ice and that linear mechanisms were sufficient to explain the observed groups. They find that the enhancement of groups is well correlated with a decrease in spectral bandwidth ν, and a decrease in wave steepness ε. The synthesis of these studies is that (i) wave groups are generally enhanced in sea ice, and (ii) nonlinear mechanisms may only be appreciable in thicker ice.

2 Methods

2.1 Observations

The Ice Profiling Sonar (IPS) is a single-beam upward-looking 420 kHz sonar commonly used to measure sea ice keels. The range r to the upper water interface, i.e. the underside of the ice, or the free surface if no ice is present, is recorded at a sampling frequency of up to 2 Hz. In addition, the water temperature T is recorded at the sensor depth with a 2-min sampling interval (Figs. 1b and 2b). Up to nine IPS were deployed from 2009 to 2014 in the Chukchi Sea as part of the multi-disciplinary, industry-sponsored Chukchi Sea Environmental Studies Program This paper focuses on the two IPS at the locations 'Crackerjack' and 'Burger' (Table 1). The distance between the mean water level and the sonar was 40 m, yielding a sonar footprint of 1.25 m at the surface. The sampling frequency varied during the yearly deployments depending on the expected ice condition, reaching 0.5 Hz or 1 Hz during the freeze-up and ice-covered periods. With these high sampling frequencies and the moderate size of the footprint, the IPS is capable of resolving surface waves. During summer months, the sampling frequency was a mix of 0.2 Hz continuous pings for ice draft measurements and 1024-s wave bursts at 2 Hz every 1.5 h. The data records with sampling frequencies < 0.5 Hz, including the short wave burst segments, are not included in the following work. In total, there are about 1400 days of data suitable for wave extraction at Crackerjack, and 1850 days at Burger (Table 1).

We convert the range data into an elevation time series:

$$\eta(t) = d(t) - \overline{d(t)}, \tag{1}$$

where $d = r\,cos\phi$ is the interface range corrected for the instrument tilt ϕ, and the overbar represents an average over the duration of the data record, which varied between a few weeks and about 2 months (Figs. 1a and 2a). Changes in the elevation η are due to changes in the surface elevation, i.e. tides and surface waves, or due to ice with varying draft drifting across the sonar beam. Our range calculations assume a constant sound speed, and temperature and salinity changes can result in additional changes in range of up to ± 0.2 m. However, these changes occur on long time scales and do not affect the following calculation of wave properties.

We split the elevation record into 20-min segments and calculate ice draft and surface elevation characteristics. For each segment, we obtain the variance spectra $P(f)$ with fixed frequency resolution independent of the sampling rate, but with varying Nyquist frequencies f_N (Figs. 1b and 2b). The spectral characteristics change drastically throughout

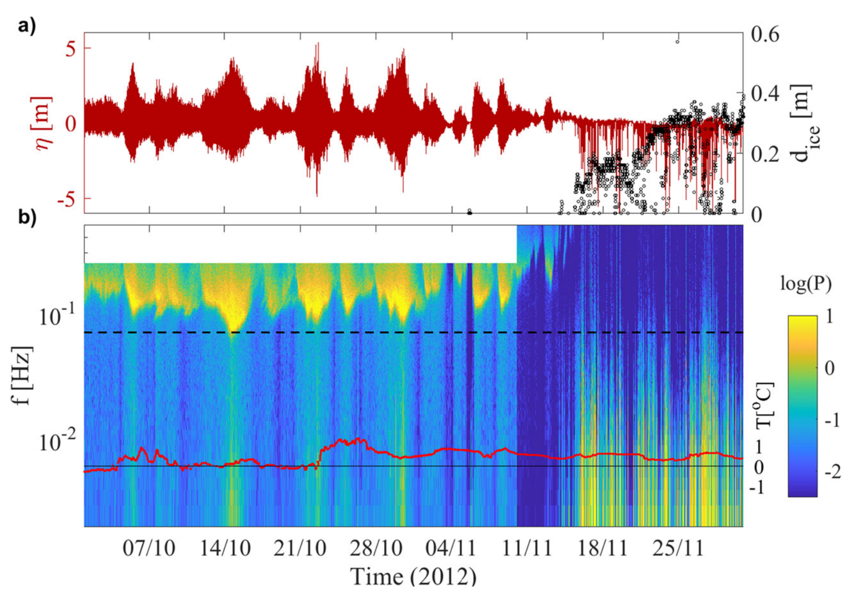

Fig. 1 Conditions during fall freeze-up at Crackerjack. **a** Surface elevation η (red line) and mean ice draft d_{ice} (black circles). **b** Spectrogram of surface elevation. Dashed line at $f = 0.07$ Hz indicates threshold for surface waves. Red line depicts temperature T at sensor depth

Fig. 2 As in Fig. 1 but for location Burger

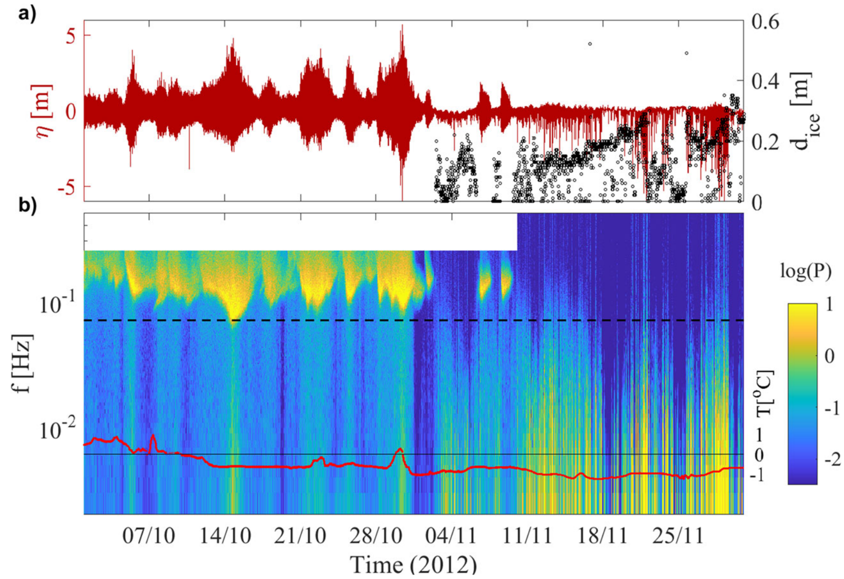

the records. During ice-free conditions, elevation changes are roughly symmetric and occur at frequencies $f > 0.07$ Hz, whereas during periods of ice cover, the elevation record is skewed towards negative values and the energy is concentrated at low frequencies $f \ll 0.05$ Hz (Figs. 1a and 2a). The spectrograms reveal bursts of energy associated with wind events of up to 2-day duration. During these events, there is a clear frequency downshift associated with a developing surface wave field. The timing of freeze-up and melting at the two locations can differ by several days, and intermediate re-opening and re-freezing is observed. Under ice cover, the high-frequency content is severely reduced and the energy is associated with drifting ice with periods of several minutes. The wave field at the two locations is fetch-limited and during ice-free conditions, no significant power is observed at frequencies below ≈ 0.07 Hz. Therefore, we define an empirical frequency threshold $f_W = 0.07$ Hz to separate surface waves at $f > f_W$, and ice roughness at $f < f_W$. This is similar to the spectral partitioning of Shcherbina et al. (2016).

In principle, small-scale ice roughness could also contribute to variance in the surface wave band. A roughness element of horizontal lengths scale L, drifting across the IPS beam at speed v, contributes to variance at frequency $f = v/L$. The mean ice drift speed, obtained from ADCP measurements at the locations, is $v_{av} = 0.16\,\mathrm{ms}^{-1}$. Taking the minimum length scale to be detected equal to twice the sonar footprint, $L_{\min} = 2.5$ m, we find the highest frequency due to ice roughness $f_{\max} = 0.064$ Hz, and thus on average the variance contribution from ice roughness is outside the wave band. However, ice drift speeds of up to $1\,\mathrm{ms}^{-1}$ have been observed. For these extreme drift speeds, ice roughness with length scales $2.5\,\mathrm{m} < L \leq 14$ m would be interpreted as surface waves.

2.2 Wave parameters

The following set of wave parameters are calculated for the entire data records and are based on 20-min elevation records. About 80% of the data were sampled at 0.5 Hz, and the remainder at 1 Hz (Table 1). Since spectral moments depend on the frequency band considered which in our case has a variable upper bound f_N, all 1-Hz resolution data are downsampled to 0.5 Hz, and $F_N = 0.25$ Hz for all data.

Spectral moments:

$$m_n = \int_{f_W}^{f_N} f^n \, P(f)\, df, \quad n = 0, 1, 2 \tag{2}$$

Significant wave height:

$$H_s = 4\sqrt{m_o} \tag{3}$$

Table 1 Deployment summary

Station name	Coordinates	Water depth	Duration	0.5-Hz sampling	1-Hz sampling
Crackerjack	71° 10.2387′ N, 166° 45.0402′ W	47.1 m	Nov 2009–May 2014	1181 days	232 days
Burger	71° 14.3976′ N, 163° 16.5923′ W	46.5m	Oct 2010–Sep 2015	1468 days	372 days

Dominant frequency (Young 1995):

$$f_p = \frac{\int_{f_W}^{f_N} f\, P(f)^4\, df}{\int_{f_W}^{f_N} P(f)^4\, df} \tag{4}$$

Bandwidth (Longuet-Higgins 1984):

$$\nu = \left(\frac{m_0 m_2}{m_1^2} - 1\right)^{\frac{1}{2}} \tag{5}$$

Wave steepness:

$$\varepsilon = k_p H_s \tag{6}$$

where the peak wavenumber k_p is obtained iteratively from the wave dispersion relation $\omega_p^2 = g k_p \tanh(k_p h)$, where h is the water depth, and $\omega_p = 2\pi f_p$.

Benjamin Feir Index:

$$\mathrm{BFI} = \sqrt{2}\, \varepsilon\, \nu^{-1} \tag{7}$$

Group factor (Funke and Mansard 1980):

$$\mathrm{GF} = \frac{\sigma(\mathrm{SIWEH})}{\langle \mathrm{SIWEH} \rangle} \tag{8}$$

where the **S**moothed **I**nstantaneous **W**ave **E**nergy **H**istory SIWEH $= Q * \eta^2$ is the convolution of the squared elevation record η^2, and a Bartlett window Q of length $2/f_p$. SIWEH is a measure of the envelope of the elevation record that is particularly well suited to provide identification of groups (Funke and Mansard 1980). The brackets $\langle\ \rangle$ indicate an average over the 20-min segments, and σ its standard deviation. For young wave fields, the length of the Bartlett window can be as short as a few data points, due to the low sampling rate of the data. This can result in unrealistic high and noisy estimates of the group factor. Therefore, for the calculation of SIWEH, we linearly interpolate the elevation record to 5-Hz sampling, which increases the resolution of the convolution, and therefore improves the group factor calculation.

2.3 Ice conditions

The Chukchi Sea undergoes a seasonal cycle of ice coverage (Serreze et al. 2016). The two locations are ice-free in early summer, freeze-up occurs towards the end of October, and at the end of winter nearly full ice cover with a mix of thin first-year ice (0.3–0.7 m) and medium first-year ice (0.7–1.2 m) are reported on weekly ice charts (www.natice.noaa.gov). In addition, we analyze the IPS data for ice draft and obtain the minimum, maximum, mean, and standard deviation for 20-min records.

Ice draft estimates are based on a combination of tilt data, acoustic range data, and pressure sensor data from the IPS along with sound speed and density measurements from CTD casts and moored CT sensors, and barometric pressure measurements provided by the nearest weather stations or numerical models (Melling et al. 1995; Fissel et al. 2008). The acoustic range data, corrected for tilt and sound speed fluctuations, provide an estimate for the distance to the sea ice or water surface during open-water events. IPS pressure data, corrected for atmospheric pressure and water density, provide an estimate of water level at all times. The difference between these two estimates yield the sea ice draft. CTD casts, and therefore density profiles, are only available at the deployment and recovery. To reduce the resulting uncertainty in the ice draft calculation ongoing inter-comparison of the two different methods is performed during open-water period. For given densities of sea water and sea ice, one can obtain the buoyancy of the ice sheet and estimate the average ice thickness. For the conditions at the two locations, the average ice thickness is roughly 10% greater than the observed ice draft.

Here, we are interested in the behaviour of waves in ice. Therefore, we restrict the following analysis to periods with well-defined surface wave action when the waveheight is above a threshold $H_s > H_{th}$. As a threshold, we choose $H_{th} = 0.2$ m, which excludes the lowest one-third of the wave observations. Tests with $H_{th} = 0.5$ m (54% excluded) and $H_{th} = 1.0$ m (75% excluded) show that the results are qualitatively insensitive to increasing the threshold. During the freeze-up and melt periods, ice conditions can vary on a daily basis and ice conditions cannot always be determined from our data. However, surface waves on ice-free and ice-infested water have different characteristics and we identify ice-free and ice-infested data segments based on a combination of following parameters:

Spectral partitioning:

$$R_m = \frac{\int_{f_W}^{f_N} P(f)\, df}{\int_{0}^{f_N} P(f)\, df}, \tag{9}$$

Surface symmetry:

$$R_s = |1 - \frac{\sigma_n}{\sigma_p}|, \tag{10}$$

where σ_n, σ_p are the standard deviation of the elevation data that are greater (smaller) than the mean elevation, respectively. Additional parameters used to identify ice are the peak period T_p, and the temperature T at the sensor depth which is coarsely related to the ice cover. As mentioned above, for fast drift speeds, ice roughness can also contribute to variance at $f > f_W$. The variance spectrum of ice roughness is generally monotonically decreasing with increasing frequency and the inferred dominant period $T_p \approx f_W^{-1}$. On the other hand, wave spectra drop off at $f < T_p^{-1}$, and the peak period $T_p < f_W^{-1}$.

For each 20-min segment with $H_s > H_{th}$, we use following criteria: [$R_m > 0.9$, $R_s < 0.2$, $T > 0^o$C] for ice-free conditions, and [$R_s > 0.2$, $T < -1.5^o$C, $T_p < 13$ s] for ice-covered segments. There is no single parameter to determine the ice conditions. For example, in ice-free wave fields, there is little low-frequency energy and $R_m \rightarrow 1$, but $R_m > 0.9$ can also occur in smooth ice conditions. The combination of the above stated thresholds provides a robust partitioning; however, it excludes all segments with $-1.5°$ C$< T > 0^{o}$C. This temperature range likely includes conditions ranging from ice-free to partial to full cover with thin ice.

In ice-covered conditions, the significant wave heights reached 3 m at Crackerjack and 4 m at Burger, whereas in ice-free conditions, the maximum value of H_s was 5 m at both locations. The dominant wave period is slightly larger in ice-covered conditions. The most common period is about 7 s and the largest period $T_p = 13$ s reflects our cut-off frequency for waves, $f \geq 0.07$ Hz (Fig. 3). These observations are consistent with recent published surface wave climatologies of the region (Francis et al. 2011; Wang et al. 2015; Thomson et al. 2016; Liu et al. 2016).

The mean ice draft d_{ice} for the data segments identified as ice-covered ranges from 0.1 m to more than 5 m (Fig. 4). At both locations, the ice draft distribution peaks at $d_{\text{ice}} \approx 0.9$ m, and values > 1.5 m are slightly more prevalent at Crackerjack. For all data segments identified as ice-free by our ice detection scheme described above, no ice is reported by the ice draft analysis, $d_{\text{ice}} = 0$, reconfirming our detection scheme.

3 Results

Overall, there are about 22,500 segments of ice-free data and 12,000 segments of ice-covered data with valid wave observations. This large data set allows us to establish potential dependencies between the groupiness of waves and the underlying wave characteristics under ice-free and ice-covered conditions. Thomson et al. (2019) found for waves propagating through new pancake ice, the wave groups are enhanced compared to conditions outside the MIZ. For these conditions, the group enhancement is well correlated with a decrease in spectral bandwidth ν, a

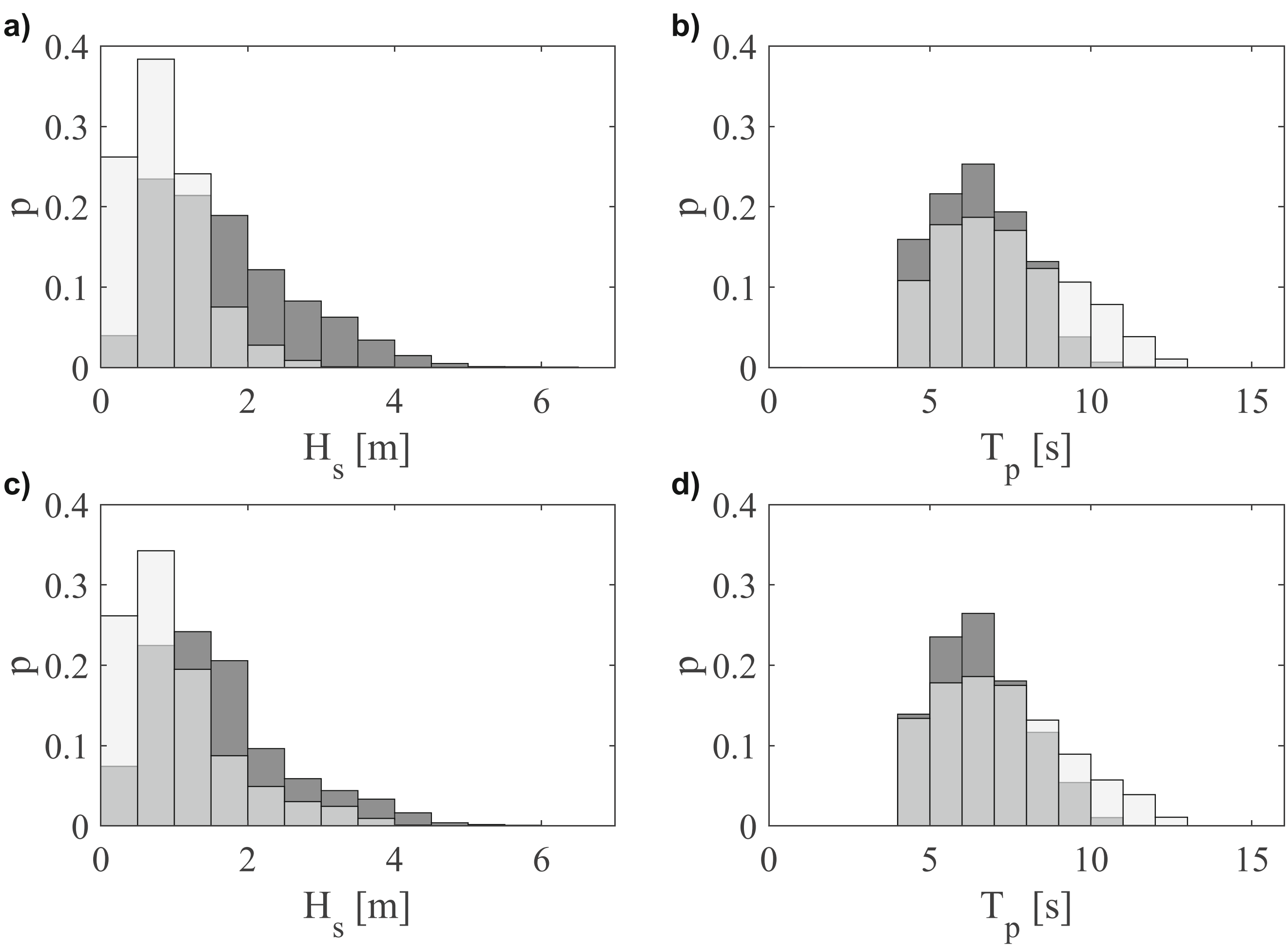

Fig. 3 Probability distribution of wave parameters at Crackerjack **a**, **b**, and Burger **c**, **d**. Dark gray bars: ice-free conditions. Light gray bars: ice-covered conditions. Left column **a**, **c**: Significant wave height H_s. Right column **b**, **d** dominant wave period T_p

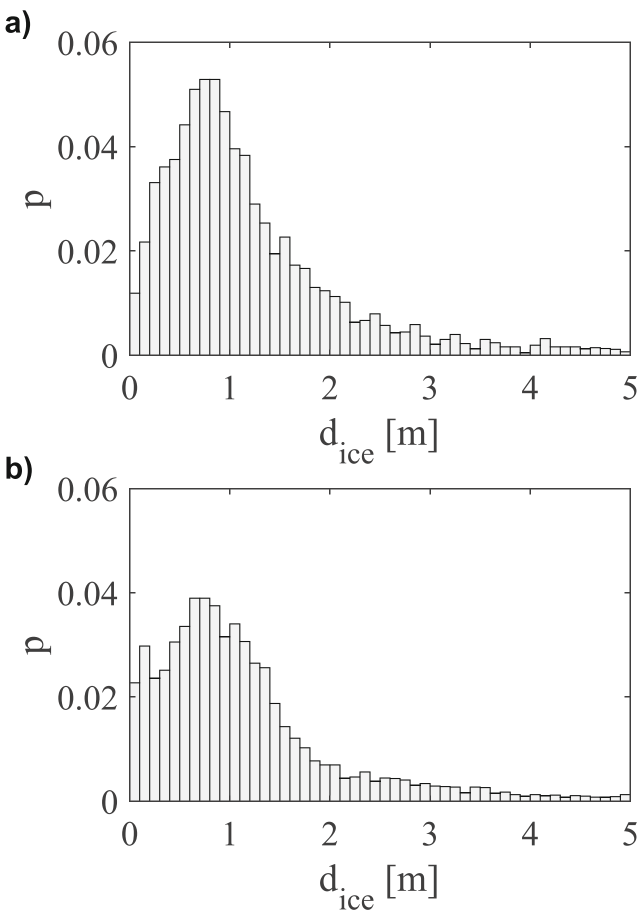

Fig. 4 Probability distribution of mean ice draft d_{ice} during data segments flagged as ice-covered. **a** At Crackerjack and **b** at Burger

decrease in wave steepness ε, and very small Benjamin Feir Index, BFI < 0.1. We perform a similar analysis as in Thomson et al. (2019). However, data in ice-free and ice-covered conditions are taken at the same location and are separated in time, whereas the data in Thomson et al. (2019) were all taken during the same storm event but at different locations. Figures 5, 6, and 8 relate the group factor GF to wave field parameters. Data from individual data segments GF, shown as gray dots, are averaged over eight equally-sized bins $\overline{GF}$, depicted as circles. Generally, wave groups are more pronounced in ice-covered conditions, where $0.8 < \overline{GF} < 1.1$, compared to ice-free wave fields where $0.7 < \overline{GF} < 0.9$. This general result is consistent with Thomson et al. (2019), who also find that waves are groupier within sea ice. The average ice draft d_{ice} within the wave parameter bins ranges from 1 to 2 m for the ice-covered conditions.

Observations in ice-free conditions show a robust positive linear trend of increasing groupiness with increasing wave steepness (Fig. 5). Increased wave steepness leads to more pronounced wave nonlinearity, and this trend is consistent with nonlinear mechanisms playing an important role in the formation of wave groups. Wave steepness in ice spans roughly the same range as in open water, but values are somewhat clustered towards low steepness. In ice, wave groupiness also shows a correlation between groupiness and wave steepness. The trend is more noisy than in the ice-free conditions but still well pronounced. More importantly, the trend is negative and groupiness decreases with increasing wave steepness. This is similar to the trend found in pancake ice, but the steepness values are notably larger here, which could also be related to the different instrumentation. At Burger, larger steepness is associated with deeper ice draft, but no such a correlation is found for Crackerjack, suggesting that in general there is no robust correlation between ice thickness at wave steepness.

When the group factor data are binned with respect to the spectral bandwidth ν, following trends emerge: for narrow-banded wave fields, $\nu \approx 0.2$, group factor values are similar in ice and ice-free condition, $\overline{GF} \approx 0.85$ (Fig. 6). However, for more broad-banded spectra, the groupiness depends on ice conditions. In ice-free conditions, the groupiness rapidly decreases as the wave field gets more broad-banded, and the group factor reduces to $\overline{GF} \approx 0.75$ for $\nu = 0.4$. In ice-covered condition, the correlation of wave groupiness and bandwidth is not that clear. In particular for $\nu > 0.3$, the group factor covers a very wide range $0.5 \lesssim GF \lesssim 1.2$ with bin averages of $\overline{GF} \approx 1.05$. Over the entire range of bandwidth an overall positive trend emerges, with increasing group factor for increasing bandwidth. This overall trend, which is opposite to the trend in ice-free conditions, is surprising and needs further analysis.

Ice is known to filter out high frequencies of the wave field which results in smaller bandwidth. Thomson et al. (2019) find the bandwidth $0.1 \leq \nu \leq 0.22$ during thin ice cover to be more narrow than during ice-free condition ($0.2 \leq \nu \leq 0.48$), and in the latter case, a clear negative trend of decreasing group factor with increasing bandwidth, similar to what we find here. For ice-covered conditions, no trend exists in the Thomson et al. (2019) study.

There are several different measure of bandwidth (for references see, e.g. Saulnier et al. (2011)) and the exact functional dependence of groupiness and bandwidth will likely depend on the specific choice of bandwidth parameter. However, differences in spectral bandwidth can readily be seen in the spectra themselves. We calculate average spectra from data recorded at Burger during the period September 2013 and August 2014 (Fig. 7). The most narrow spectrum corresponds to ice-free conditions. In comparison, the average spectrum for ice-covered condition has much higher low-frequency variance and a weaker decay at frequencies above the dominant frequency. This results in a slightly larger average bandwidth, consistent with the higher upper bound of of individual ν—values seen in Fig. 6. The average spectrum of narrow-banded ($\nu < 0.3$) ice-covered wave fields

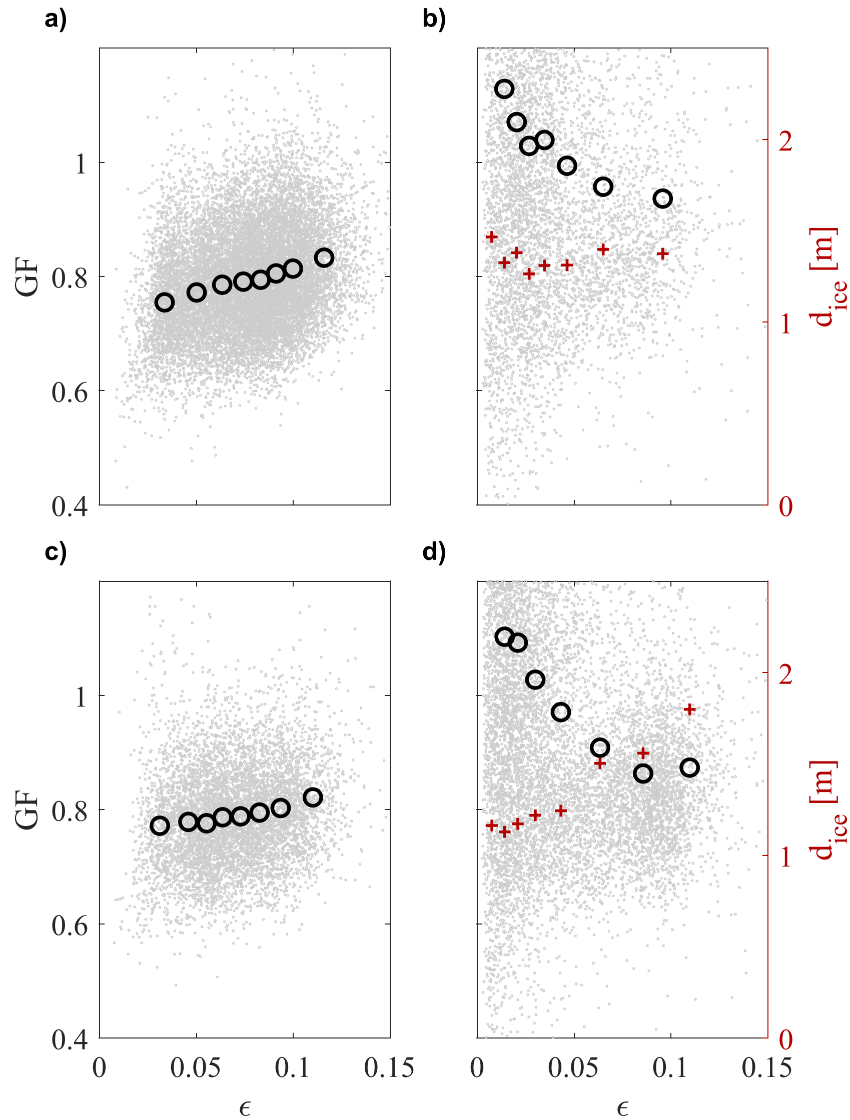

Fig. 5 Group factor GF (black circles, and gray dots), and mean ice draft d_{ice} (red crosses) as function of wave steepness ϵ, at Crackerjack **a**, **b**, and Burger **c**, **d**. Left column **a**, **c**: for ice-free conditions. Right column **b**, **d** for ice-covered conditions

is nearly identical to that for ice-free conditions, except slightly higher variance at the lowest frequencies in the wave band. In this bandwidth, range the group factor is also similar in ice-covered and ice-free conditions (Fig. 6). The large bandwidth range $\nu > 0.3$ is only found for waves in ice. The average spectrum for these conditions shows a dominant wave frequency $f_p \approx 0.08$ Hz much lower than for the narrow-banded wave fields ($f_p \approx 0.12$ Hz). At frequencies above the spectral peak, spectral levels fall off rapidly but stay nearly level at $f \gtrsim 0.13$Hz. It is this broad high-frequency tail that causes the large bandwidth values. However, the physical origin of these high variance levels could be due to surface waves, or increased noise in the observations, and the extreme large bandwidth values could be contaminated by high-frequency noise. If the large bandwidth values are based on surface waves, this suggests that the observed wave events are locally generated, rather than waves that have propagated for long distances through ice. The mean ice draft does not correlate with bandwidth.

To further assess if wave groupiness is associated with nonlinearity, we bin the group factor in terms of the Benjamin-Feir Index. For ice-free waters, there is a very clear trend of increasing groupiness with increasing BFI (Fig. 8). Since BFI is the ratio between wave steepness and bandwidth (Eq. 7), the well-defined trend reflects the high correlations of group factor with wave steepness and bandwidth (Figs. 5 and 6). The BFI values range from 0.1 to $\approx$ 1, the critical value for the onset of the Benjamin-Feir instability. The positive trend indicates that in open water nonlinearity is likely an important factor for wave groupiness in the Chukchi Sea. For wave fields in ice, the BFI values are generally smaller than in open water conditions, and there are noticeable differences at the two locations. At Crackerjack, two-thirds of the data

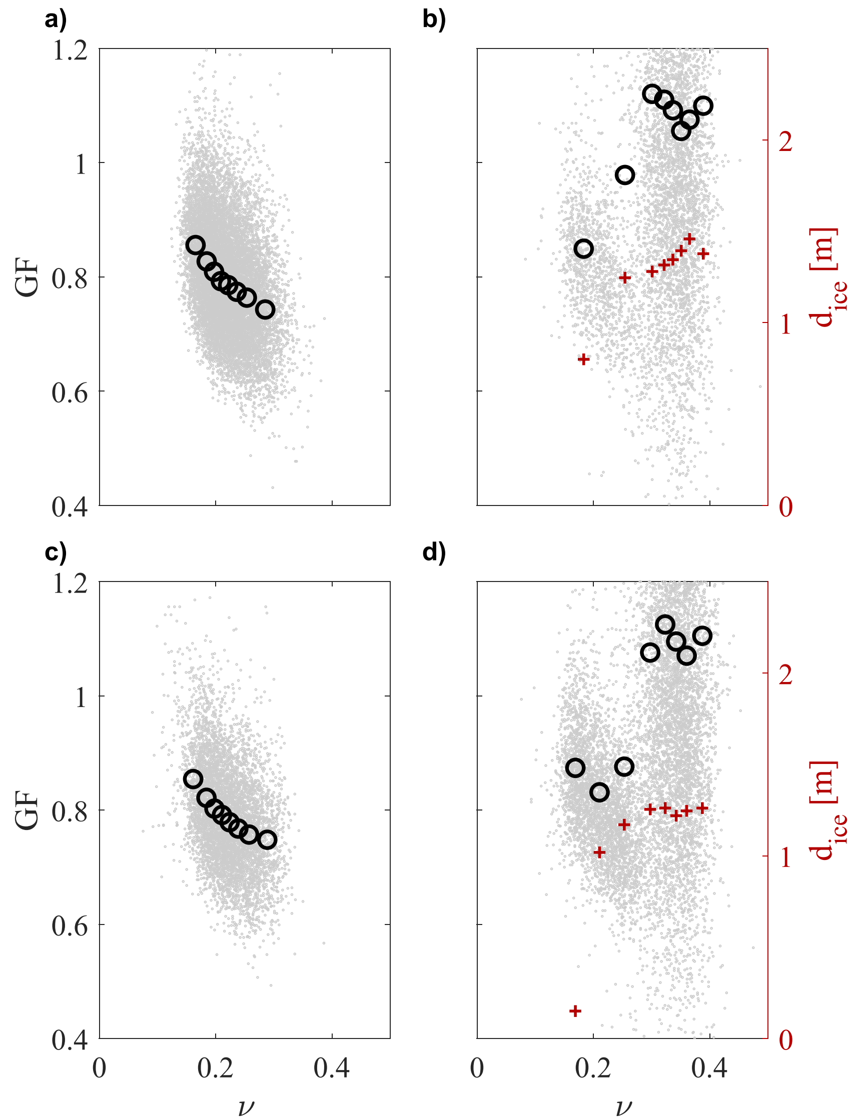

Fig. 6 Group factor GF (black circles, and gray dots), and mean ice draft d_{ice} (red crosses) as function of spectral bandwidth ν, at Crackerjack **a**, **b**, and Burger **c**, **d**. Left column **a**, **c**: for ice-free conditions. Right column **b**, **d** for ice-covered conditions

have BFI<0.3 and there is a well-established negative trend of decreasing groupiness with increasing BFI. At Burger, about half the data are at BFI<0.3 and show a strong negative trend with the group factor. There is some indication of a reversal of the trend at higher BFI values. Taking all data, the trend is negative, i.e. decreasing groupiness with increasing BFI, consistent with the trend at Crackerjack. The mean ice draft d_{ice} binned by BFI values is also different at the two locations. At Crackerjack, the ice draft is uncorrelated with BFI whereas at Burger, there is a clear positive trend with deeper ice draft associated with higher BFI.

4 Discussion

Wave groups are prominent in both open water and under ice cover, at both locations. We find well-defined trends between groupiness and various parameters commonly used as indicators for wave field nonlinearity. In open water, groupiness increases with (i) increasing wave steepness, (ii) decreasing bandwidth, and (iii) increasing BFI. These are all clear indications that nonlinearity plays an important role in the development of wave groups. The wave data in open waters are largely from short wind events. Furthermore, the observations were taken in the eastern Chukchi Sea, and therefore the waves are expected to be duration and fetch limited. These young wave fields are steep and likely have a narrow directional spreading. Both factors are favourable for pronounced nonlinearity, as can also be seen in the relative high BFI values.

On the other hand, wave groups in ice seem to be inhibited by increasing nonlinearity. Groupiness in ice decreases with (i) increasing wave steepness, (ii) decreasing bandwidth, and (iii) increasing BFI. These trends are opposite to the trends found at the same locations in open water, and the correlations (i) and (iii) are significant and robust. The decrease of groupiness with decreasing bandwidth is unexpected but might be somewhat affected by an increased noise floor in the data. Linear superposition and nonlinear focusing both would lead to the opposite trend, i.e. increasing groupiness with decreasing bandwidth. However, this apparent reversal of the trend might be related to the way the nonlinearity parameters are calculated neglecting any effects of directional spreading of the wave field.

4.1 Directional considerations

The wave steepness (Eq. 6), spectral bandwidth (Eq. 5), and BFI (Eq. 7) are based on properties of nondirectional wave spectra. However, the generation of wave groups mainly depends on the spectral properties of waves aligned with the direction of the dominant waves. For example, two aligned wave trains of similar frequency generate well-defined groups, whereas the same wave trains in a crossing sea would result in a regular pattern of sea cusps, but no groups. Similarly, a spectrally broad-banded wave field generally has a weak group structure. However, if the same wave field has a broad directional spreading, it can become spectrally narrow-banded near the dominant waves. This is illustrated with two synthetic spectra with identical one-dimensional spectral shape but different directional spreading (Fig. 9). The spectra were generated with the MATLAB toolbox DIWASP (DIWASP 2012) as a superposition of one dominant spectrum and 20 spectra of increasing peak frequency, increasing directional spread, and decreasing wave energy. For the narrow directional 2-D spectrum, the direction of all individual waves is 90°. The broad spectrum consists of the dominant spectrum with direction 90° and the directions of the high-frequency spectra increase from 90° ± 30° to 90° ± 90°. Integrating the two spectra over all directions yields identical 1-D spectra (Fig. 9), and therefore identical nonlinearity parameters $\varepsilon = 0.075$ and $\nu = 0.463$. However, in the direction of the dominant waves, the spectra are obviously different. Integration of the 2-D spectra over the range 90° ± 15° yields a spectrally broad-banded 1-D spectrum for the case of a narrow directional spread, with $\varepsilon = 0.071$ and $\nu = 0.444$, but a narrower spectral bandwidth $\nu = 0.409$ and smaller steepness $\varepsilon = 0.027$ for the directional broad spectrum. Thus, linear superposition of waves propagating in the main direction will result in enhanced groupiness for the spectrum where the high-frequency components are propagating in an oblique direction. Here we hypothesize that the presence of ice modifies the directional spreading of a wave field in a manner to reduce the spectral bandwidth of the dominant waves and thus leads to the observed enhanced group structure of waves in ice. Our surface elevation records are nondirectional and we cannot test this hypothesis directly with our data. However, there is some theoretical and observational support for it.

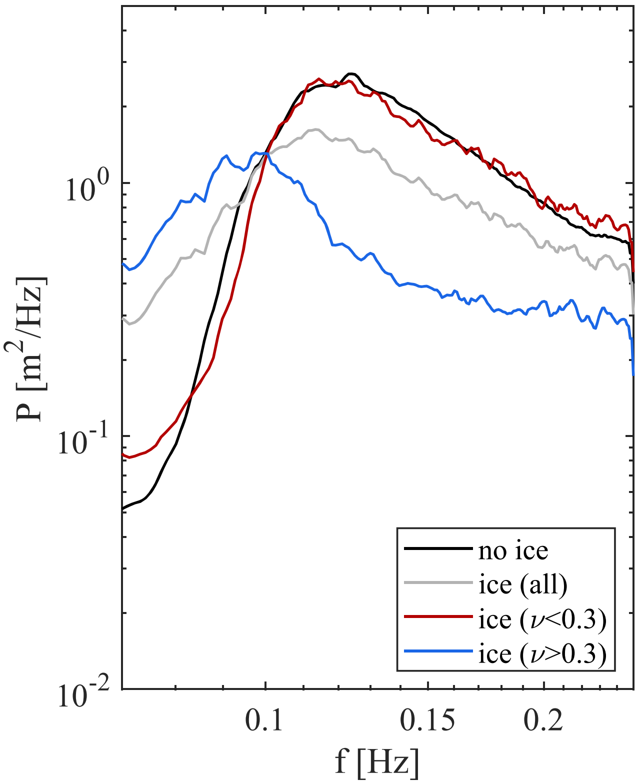

Fig. 7 Average wave height spectrum for the period 01/09/2013 to 05/08/2014 at station Burger. Black line: ice-free conditions; gray line: all ice-covered conditions, red line: ice-covered conditions with narrow bandwidth, blue line: ice-covered condition with broad bandwidth

Observations of the directional spreading of waves in ice are challenging and rare, especially at high wave numbers. Sutherland and Gascard (2016) used airborne scanning lidars in the Beaufort Sea to obtain the directional wave spectra over a flight path from the ice edge to about 60 km into the MIZ. At the dominant wavenumber, $k_p = 0.05$ rad/m, the spectral spread remained constant at $\approx 29^o$ up to 50 km into the ice, whereas at $k = 0.09$ rad/m, the spread increased from 30 to 45°. On the other hand, Montiel et al. (2018) used wave buoy observations and suggested 'that directional spreading decreases with distance of propagation in the pancake icecover, most likely as a result of directional filtering from dissipative processes'.

Polnikov and Lavrenov (2007) performed numerical calculations of the nonlinear energy transfer of surface waves on water covered with broken ice. The floating ice adds inertia, incorporated in the 'mass-loading' dispersion relation (Squire et al. 1995):

$$\omega^2 = \frac{k\, g\, \tanh(kD)}{1 + \rho_i/\rho_w\, h\, k \tanh(kD)} \tag{11}$$

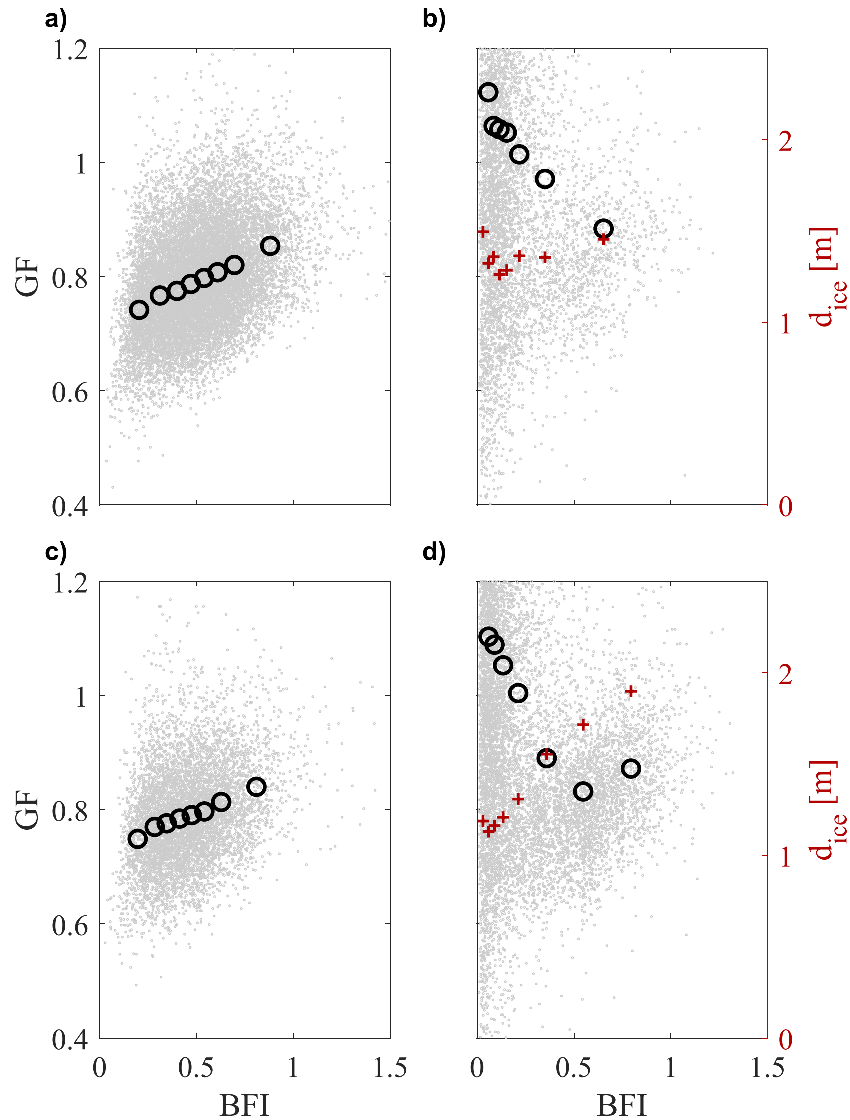

Fig. 8 Group factor GF (black circles and gray dots), and mean ice draft d_{ice} (red crosses) as function of Benjamin-Feir Index (BFI), at Crackerjack **a**, **b**, and Burger **c**, **d**. Left column **a**, **c**: for ice-free conditions. Right column **b**, **d** for ice-covered conditions

where D is the water depth, ρ_i, ρ_w are the densities of ice and water, respectively, and h is the thickness of the ice floats. They find the four-wave interaction are modified by the presence of ice and the severity of the modifications increase with increasing ice thickness, i.e. with increasing deviation of the dispersion relation from the open water dispersion relation. Overall, ice reduces the nonlinear four-wave transfer but enhances the transfer to high frequencies. On the other hand, ice is known to act as a lowpass filter on waves due to mechanical damping (Collins et al. 2017). The enhanced nonlinear transfer at high frequencies acts against this damping. If the nonlinear transfer fully counteracts the damping, the spectral bandwidth in ice covered conditions spans the same range of values as that in open water, which is consistent with our observations (Fig. 6). The reduction of high-frequency wave energy occurs even in thin frazil ice (Rogers et al. 2016; Cheng et al. 2017) whereas the enhanced nonlinear transfer is most effective in thicker ice. Thomson et al. (2019) find vastly different bandwidth values in pancake ice, $0.1 < \nu < 0.2$ compared to $0.2 < \nu < 0.5$ in water. This is consistent with no enhanced nonlinear transfer in thin ice, but the lower frequency resolution of their observations in ice might also contribute to this difference.

Furthermore, Polnikov and Lavrenov (2007) find that the high-frequency energy spreads to lateral directions, thus making the waves in the dominant direction more narrow-banded, as discussed above. Therefore, the enhanced high-frequency nonlinear transfer in ice can in principle lead to an increased group factor. This might be part of the explanation why generally the group factor in ice is larger than that in open water (Figs. 5, 6, and 8). The calculations also show that the change to the nonlinear transfer is less pronounced in narrow-banded spectra. This would mean that the directional spreading is also reduced and an overall narrow-banded wave field can actually be more

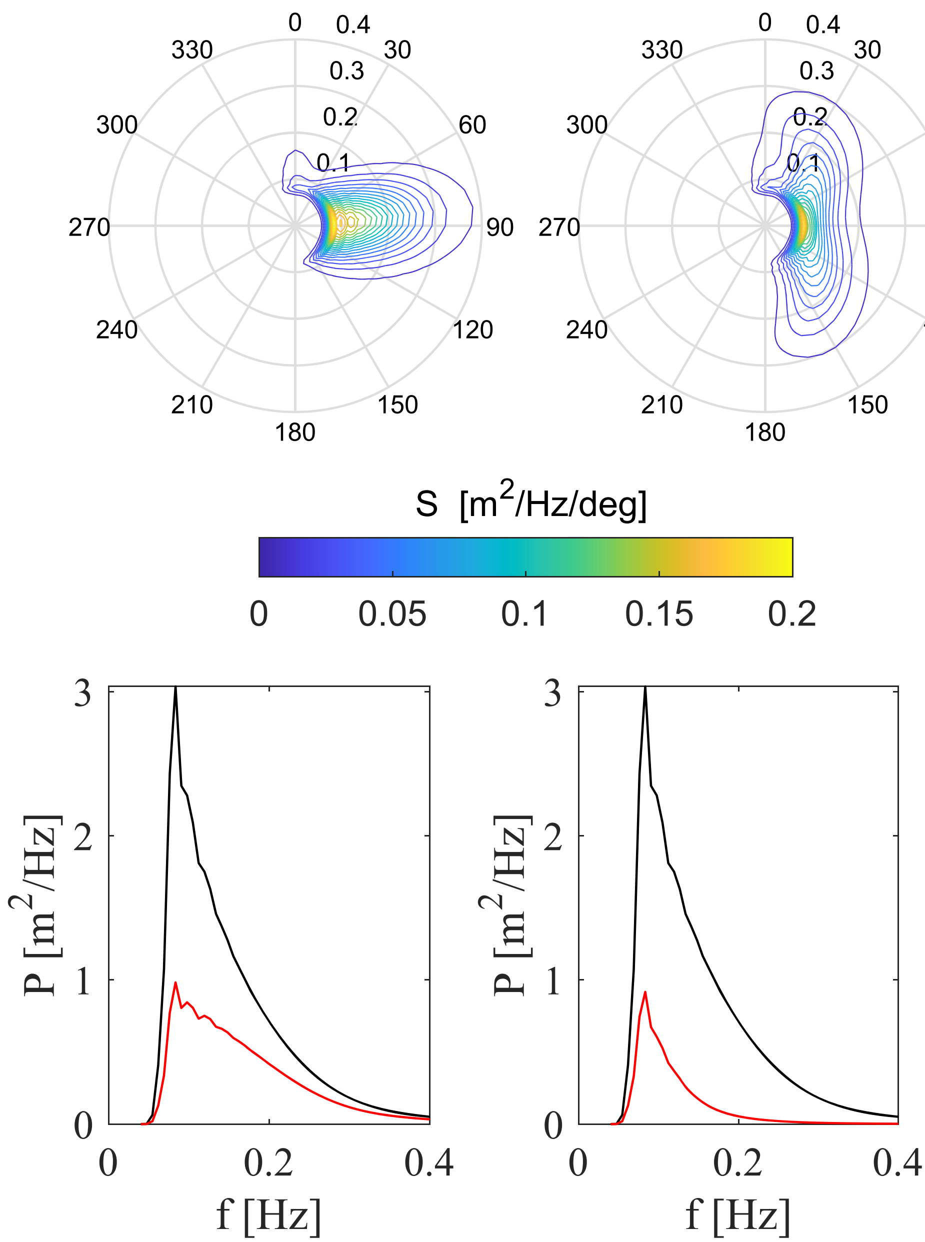

Fig. 9 Spectra of synthesized wave data. Left column: narrow directional spreading. Right column: broad directional spreading. Top row: 2-D spectra. Bottom row: 1-D spectra obtained from all directions (black) and from directions 75 to 105° only (red)

broad-banded around the dominant direction, which is the relevant parameter to affect the wave groupiness. This is consistent with the observed trends of smaller group factor for narrower bandwidth (Fig. 6b, d) and decreased group factor for larger BFI (Fig. 8b, d). In open water, wave steepness and bandwidth are uncorrelated (Fig. 10a, c). However, in ice-covered conditions, wave steepness rapidly decreases with bandwidth (Fig. 10b, d). This trend can also explain the observed negative trends of decreasing group factor with increasing wave steepness (Fig. 5b, d). Alternatively, the advection of small-scale ice roughness elements would increase steepness ε. Since ice roughness would be uncorrelated with wave motion, this would reduce groupiness, also resulting in a negative trend between ε and GF. However, small-scale ice roughness would increase the bandwidth as well as steepness, yielding a positive trend between ν and ε, contrary to our observations.

The enhanced nonlinear transfer, additional wave damping, and increased directional spreading all affect the high-frequency range of the spectrum and are absent in open water and weak in thin ice. Therefore, under those conditions, the trends are opposite to the trends in water covered with thick ice. During ice-free conditions, the wave field at the two locations in the eastern Chukchi Sea have a narrow directional spreading and superposition of wave trains yield more pronounced wave groups for narrow-banded spectra, as observed (Fig. 6a, c). On the other hand, steeper wave fields imply enhanced nonlinearity and the observed

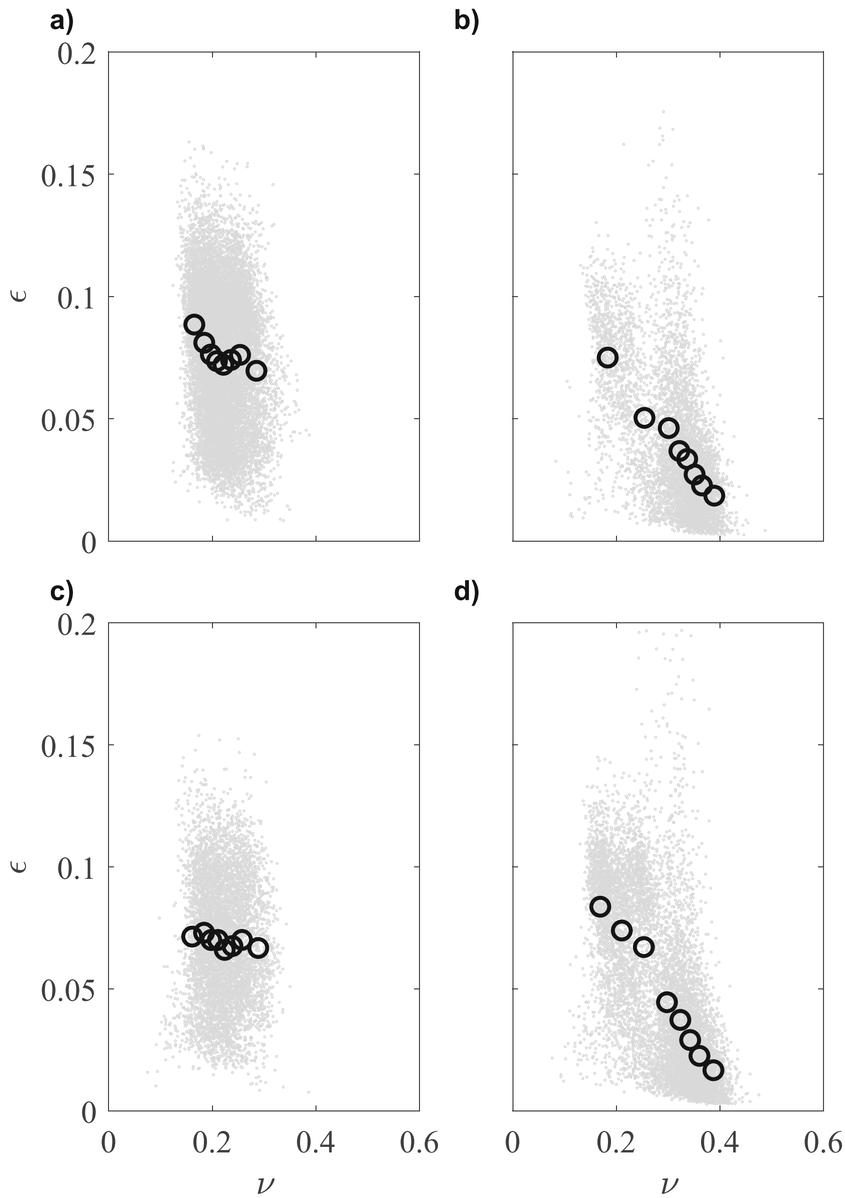

Fig. 10 Wave steepness ε as function of bandwidth ν, at Crackerjack **a**, **b**, and Burger **c**, **d**. Left column **a**, **c**: for ice-free conditions. Right column **b**, **d** for ice-covered conditions

increase in groupiness suggest that nonlinear focusing plays an important role in the generation of wave groups. This is also consistent with the positive trend between group factor and BFI (Fig. 8a, c)

5 Conclusions

Wave groups are a common feature of the waves in the eastern Chukchi Sea, in ice-free and in ice-covered conditions. In general, we find that groups are more prominent in ice. We find that both the mechanisms of linear superposition and nonlinear interactions are likely contributing factors in the generation of wave groups. In open water, narrow-banded wave fields show enhanced groupiness, relative to broad-banded wave field due to their favourable conditions of phase coherent linear superposition. The observed increase of the group factor for increasing wave steepness suggests nonlinear focusing also plays an important role. Thin to medium first-year ice appears to affect the nonlinear four-wave interaction of wave energy transfer within the spectrum. The energy transfer to high-frequency waves may be enhanced and spread to directions lateral to the dominant wave direction. This modified transfer does not affect the nonlinearity parameters ε, ν, and BFI obtained from the directionally-integrated spectrum. However, the generation of wave groups is determined by the spectral shape of the waves propagating in the dominant direction, only. The effective bandwidth, calculated from the spectrum integrated over a small sector around the dominant direction only, reduces as the transfer and directional spreading of the high-frequency waves increases. This process of narrowing the effective bandwidth is most effective in broad-banded spectra. Thus, enhanced nonlinear transfer can modify the spectra in a way that lead to enhanced group generation by linear superposition. However, increased high-frequency noise in the observations would also be consistent with an increased omni-directional bandwidth. Long-term high-quality observations of directional wave spectra, as opposed to the scalar measurements herein, would be required to asses more completely the hypothesis of modified nonlinear transfer leading to enhanced groupiness in ice.

Acknowledgements The data were originally collected for Shell Exploration and Production as part of the Chukchi Sea Environmental Studies Program. We thank Keath Borg (ASL) for support in the initial IPS data processing and providing high-resolution ice draft statistics.

Funding Funding was provided by the Natural Sciences and Engineering Council of Canada (NSERC) as part of the ENGAGE program.

Compliance with ethical standards

Conflict of interest The authors declare that they have no conflict of interest.

References

Banner ML, Pierson WL (2007) Wave breaking onset and strength for two-dimensional deep water wave groups. J. Fluid Mech. 585:93–115

Benjamin TB, Feir J (1967) The disintegration of wave trains on deep water part 1. J. Fluid Mech. 27(03):417–430

Cheng S et al (2017) Calibrating a viscoelastic sea ice model for wave propagation in the arctic fall marginal ice zone. Journal of Geophysical research: Oceans 122:n/a–n/a. https://doi.org/10.1002/2017JC013275

Collins CO, Rogers WE, Marchenko A, Babanin AV (2015) In situ measurements of an energetic wave event in the arctic marginal ice zone. Geophysical Research Letters, pp n/a–n/a. https://doi.org/10.1002/2015GL063063

Collins CO, Rogers WE, Lund B (2017) An investigation into the dispersion of ocean surface waves in sea ice. Ocean Dynamics 67:263–280. https://doi.org/10.1007/s10236-016-1021-4

DIWASP DIWASP (2012) A directional wave spectra toolbox for MATLAB: user manual. Research report WP-1601-DJ, Tech. rep., Centre for Water Research, University of Western Australia

Elgar S, Guza RT, Seymour RJ (1984) Groups of waves in shallow water. J Geophys. Res. 89(C3):3623–3634

Fissel D, Marko J, Melling H (2008) Advances in upward looking sonar technology for studying the processes of change in arctic ocean ice climate. Journal of Operational Oceanography 1(1):9–18. https://doi.org/10.1080/1755876x.2008.11081884

Francis OP, Panteleev GG, Atkinson DE (2011) Ocean wave conditions in the Chukchi Sea from satellite and in situ observations. Geophys Res Lett, 38(L24610), 5pp. https://doi.org/10.1029/2011GL049839

Funke ER, Mansard EPD (1980) On the synthesis of realistic sea states. In: Proceedings of the international conference on coastal engineering, pp 2974–2991

Gemmrich J, Thomson J (2017) Observations of the shape and group dynamics of rogue waves. Geophysical Research Letters 44(4):1823–1830. https://doi.org/10.1002/2016GL072398. 2016GL072398

Liu AK, Mollo-Christensen E (1988) Wave propagation in a solid ice pack. J Phys Oceanogr 18(11):1702–1712

Liu Q, Babanin AV, Zieger S, Young IR, Guan C (2016) Wind and wave climate in the arctic ocean as observed by altimeters. Journal of Climate 29(22):7957–7975. https://doi.org/10.1175/JCLI-D-16-0219.1

Longuet-Higgins MS (1984) Statistical properties of wave groups in a random sea state. Philosophical Transactions of the Royal Society of London Series A 312:219–250

Melling H, Johnston PH, Riedel DA (1995) Measurements of the underside topography of sea ice by moored subsea sonar. Journal of Atmospheric and Oceanic Technology 12(3):589–602. https://doi.org/10.1175/1520-0426(1995)012⟨0589:motuto⟩2.0.co;2

Meylan MH, Bennetts LG, Mosig JEM, Rogers WE, Doble MJ, Peter MA (2018) Dispersion relations, power laws, and energy loss for waves in the marginal ice zone. Journal of Geophysical Research: Oceans 123(5):3322–3335. https://doi.org/10.1002/2018JC013776

Montiel F, Squire VA, Doble M, Thomson J, Wadhams P (2018) Attenuation and directional spreading of ocean waves during a storm event in the autumn Beaufort Sea marginal ice zone. Journal of Geophysical Research: Oceans 0(0):5912–5932. https://doi.org/10.1029/2018JC013763

Polnikov VG, Lavrenov IV (2007) Calculation of the nonlinear energy transfer through the wave spectrum at the sea surface covered with broken ice. Oceanology 47(3):363–373. https://doi.org/10.1134/s0001437007030058

Rogers WE, Thomson J, Shen HH, Doble MJ, Wadhams P, Cheng S (2016) Dissipation of wind waves by pancake and frazil ice in the autumn Beaufort Sea. Journal of Geophysical Research: Oceans 121(11):7991–8007. https://doi.org/10.1002/2016JC012251

Saulnier J-B, Clément A, de O. Falcão AF, Pontes T, Prevosto M, Ricci P (2011) Wave groupiness and spectral bandwidth as relevant parameters for the performance assessment of wave energy converters. Ocean Engineering 38(1):130–147. https://doi.org/10.1016/j.oceaneng.2010.10.002

Serreze MC, Crawford AD, Stroeve JC, Barrett AP, Woodgate RA (2016) Variability, trends, and predictability of seasonal sea ice retreat and advance in the Chukchi Sea. Journal of Geophysical research: oceans, pp n/a–n/a

Shcherbina AY, McNeil CL, Baptista AM (2016) Model-aided lagrangian interpretation of non-synoptic estuarine observations. Limnology and oceanography: methods, pp. n/a–n/a

Shen HH, Squire VA (1998) Wave damping in compact pancake ice fields due to interactions between pancakes. Antaractic research series 74:325–341

Squire VA, Dugan JP, Wadhams P, Rottier PJ, Liu AK (1995) Of ocean waves and sea ice. Annual Review of Fluid Mechanics 27(1):115–168. https://doi.org/10.1146/annurev.fl.27.010195.000555

Sullivan PP, Banner ML, Morison RP, Peirson WL (2018) Turbulent flow over steep steady and unsteady waves under strong wind forcing. Journal of Physical Oceanography 48(1):3–27. https://doi.org/10.1175/JPO-D-17-0118.1

Sutherland P, Gascard J-C (2016) Airborne remote sensing of ocean wave directional wavenumber spectra in the marginal ice zone. Geophysical Research Letters, 43(10). https://doi.org/10.1002/2016gl067713

Thomson J, Gemmrich J, Rogers WE, Collins CO, Ardhuin F (2019) Wave groups observed in pancake sea ice. Journal of Geophysical Research: Oceans 124(11):7400–7411. https://doi.org/10.1029/2019jc015354

Thomson J et al (2016) Emerging trends in the sea state of the Beaufort and Chukchi Seas. Ocean Modelling 105:1–12. https://doi.org/10.1016/j.ocemod.2016.02.009

van den Bremer TS, Taylor PH (2015) Estimates of Lagrangian transport by surface gravity wave groups: the effects of finite depth and directionality. Journal of Geophysical research: Oceans. https://doi.org/10.1002/2015JC010712

Wang XL, Feng Y, Swail VR, Cox A (2015) Historical changes in the Beaufort-Chukchi-Bering Seas surface winds and waves. 1971–2013, Journal of Climate

Young I (1995) The determination of confidence limits associated with estimates of the spectral peak frequency. Ocean Engineering 22(7):669–686. https://doi.org/10.1016/0029-8018(95)00002-3